

# On the origin of cold-dense plasmas in the dusk magnetotail plasma sheet: MMS Observations

Masaki N Nishino<sup>1,1</sup>, Yoshifumi Saito<sup>1,1</sup>, Hiroshi Hasegawa<sup>2,2</sup>, Naritoshi Kitamura<sup>3,3</sup>, Yukinaga Miyashita<sup>4,4</sup>, Tsugunobu Nagai<sup>1,1</sup>, shoichiro yokota<sup>5,5</sup>, Daniel J Gershman<sup>6,6</sup>, Christopher T. Russell<sup>7,7</sup>, and Barbara L. Giles<sup>6,6</sup>

<sup>1</sup>Institute of Space and Astronautical Science, Japan Aerospace Exploration Agency

<sup>2</sup>Institute of Space and Astronautical Science

<sup>3</sup>The University of Tokyo

<sup>4</sup>Korea Astronomy and Space Science Institute

<sup>5</sup>Osaka University

<sup>6</sup>NASA Goddard Space Flight Center

<sup>7</sup>University of California Los Angeles

November 30, 2022

## Abstract

The near-Earth plasma sheet becomes cold and dense under northward interplanetary magnetic field (IMF) condition, which suggests efficient solar wind plasma entry into the magnetosphere across the magnetopause for northward IMF and a possible contribution of ionospheric oxygen ion outflow. The cold and dense characteristics of the plasma sheet are more evident in the magnetotail flank regions that are the interface between cold solar wind plasma and hot magnetospheric plasma. Several physical mechanisms have been proposed to explain the solar wind plasma entry across the magnetopause and resultant formation of the cold-dense plasma sheet (CDPS) in the tail flank regions. However, the transport path of the cold-dense plasma inside the magnetotail has not been understood yet. Here we present a case study of the CDPS in the dusk magnetotail by Magnetospheric Multiscale (MMS) spacecraft under strongly northward IMF and high-density solar wind conditions. The ion distribution function consists of high- and low-energy components, and the low-energy one intermittently shows energy dispersion in the directions parallel and anti-parallel to the local magnetic field. The time-of-flight analysis of the energy-dispersed low-energy ions suggests that these ions originate in the region farther down the tail, move along the magnetic field toward the ionosphere and then come back to the magnetotail by the mirror reflection. The pitch-angle dispersion analysis gives consistent results on the traveling time and path length of the energy-dispersed ions. Based on these observations, we discuss possible generation mechanisms of the energy-dispersed structure of the low-energy ions during the northward IMF.

# Transport path of cold-dense plasmas in the dusk magnetotail plasma sheet: MMS Observations

M. N. Nishino<sup>1</sup>, H. Hasegawa<sup>1</sup>, Y. Saito<sup>1</sup>, N. Kitamura<sup>2</sup>, Y. Miyashita<sup>3,4</sup>, T. Nagai<sup>1</sup>, S.  
Yokota<sup>5</sup>, C. T. Russell<sup>6</sup>, D. J. Gershman<sup>7</sup>, B. L. Giles<sup>7</sup>

<sup>1</sup>Institute of Space and Astronautical Science, Japan Aerospace Exploration Agency

<sup>2</sup>Graduate School of Science, The University of Tokyo, Japan

<sup>3</sup>Korea Astronomy and Space Science Institute, South Korea

<sup>4</sup>Department of Astronomy and Space Science, Korea University of Science and Technology, Daejeon, South Korea

<sup>5</sup>Graduate School of Science, Osaka University, Japan

<sup>6</sup>University of California, Los Angeles

<sup>7</sup>Goddard Space Flight Center, NASA

## Key Points:

- MMS observed the cold-dense plasma sheet in the dusk magnetotail under strongly northward IMF.
- Energy dispersions of field-aligned and anti-field-aligned streaming low-energy ions were identified.
- These ions were injected from tailside regions of the MMS location and moved along the magnetic field.

---

Corresponding author: Masaki N. Nishino, [nishino@stp.isas.jaxa.jp](mailto:nishino@stp.isas.jaxa.jp)

## Abstract

The near-Earth plasma sheet becomes cold and dense under northward interplanetary magnetic field (IMF) condition, which suggests efficient entry of solar wind plasma into the magnetosphere across the magnetopause for northward IMF and a possible contribution of the ionospheric oxygen ion outflow. The cold and dense characteristics of the plasma sheet are more evident in the magnetotail flank regions that are the interface between cold solar wind plasma and hot magnetospheric plasma. Several physical mechanisms have been proposed to explain the entry of solar wind plasma across the magnetopause and resultant formation of the cold-dense plasma sheet (CDPS) in the tail flank regions. However, the transport path of the cold-dense plasma inside the magnetotail has not been understood yet. Here we present a case study of the CDPS in the dusk magnetotail by Magnetospheric Multiscale (MMS) spacecraft under the conditions of strongly northward IMF and high-density solar wind. The ion distribution function consists of high- and low-energy components, and the low-energy one intermittently shows energy dispersion in the directions parallel and anti-parallel to the local magnetic field. The time-of-flight analysis of the energy-dispersed low-energy ions suggests that these ions originate in the region farther down the tail, and move along the magnetic field toward the ionosphere and then come back to the magnetotail by the mirror reflection. The pitch-angle dispersion analysis gives consistent results on the traveling time and path length of the energy-dispersed ions. Based on these observations, we discuss possible generation mechanisms of the energy-dispersed structure of the low-energy ions during the northward IMF.

## 1 Introduction

The plasma sheet in the Earth's magnetosphere is an important target of magnetospheric physics, since it is strongly related to geomagnetic activities through its role as the plasma reservoir. Previous research has revealed that the near-Earth plasma sheet becomes cold and dense under the northward interplanetary magnetic field (IMF) (e.g., Borovsky et al., 1998; Nagata et al., 2008; Nishino et al., 2002; Terasawa et al., 1997; Wing et al., 2005; Zwolakowska et al., 1992; Zwolakowska & Popielawska, 1992). The formation of the cold-dense plasma sheet (CDPS) has been thought as a result of solar wind entry across the magnetopause and subsequent plasma transport inside the magnetotail.

Several mechanisms have been proposed to explain the solar wind plasma entry across the magnetopause under the northward IMF, and some of them have been verified. In particular, under the strongly northward IMF condition, double-lobe reconnection (also known as magnetic reconnection poleward of the cusp) (e.g., Allen et al., 2016; Li et al., 2005; Song & Russell, 1992; Sorathia et al., 2019) and Kelvin-Helmholtz instability (e.g., Allen et al., 2016; Fairfield et al., 2000; Hasegawa et al., 2004; Sorathia et al., 2019) play an important role in solar wind plasma entry across the magnetopause. The solar wind entry across the magnetopause results in the formation of the low-latitude boundary layer (LLBL) filled with cold and dense plasma, and it possibly forms the CDPS in a wide region of the near-Earth magnetotail.

On the other hand, the plasma transport mechanism inside the magnetosphere under the northward IMF has not been well understood. Since the plasma flow in the near-Earth magnetotail under the northward IMF should reflect the transport mechanism of the cold-dense plasma, it is important to investigate the plasma flow velocity in the plasma sheet. Statistically, ion flows in the near-Earth plasma sheet during the geomagnetically quiet periods are quite stagnant with a slight earthward component (e.g., Angelopoulos et al., 1993). For most of the time, the ions in the CDPS adjacent to the LLBL slowly flow towards the Earth (Fujimoto et al., 1998).

The response time of the near-Earth plasma sheet to the solar wind during the northward IMF is confirmed to be longer than that during the southward IMF (e.g., Nagata et al., 2008). Based on the longer duration ( $\sim$ several hours) of the CDPS formation and the

low bulk velocity in the near-Earth plasma sheet under the northward IMF, diffusive transport in the plasma sheet has been proposed as a dominant mechanism in the magnetotail (Nagata et al., 2008; Terasawa et al., 1997; Wang et al., 2010). However, the CDPS occasionally appears in the midnight region only a few hours after the start of the strongly northward IMF period (Nishino, Fujimoto, Terasawa, et al., 2007), which suggests that non-diffusive plasma transport may work in the plasma sheet under the northward IMF.

In this paper we report on energy-dispersed low-energy ions in the field-aligned directions observed by the Magnetospheric Multiscale (MMS) mission spacecraft in the near-Earth magnetotail on the duskside under the strongly northward IMF. We will discuss possible mechanisms for generating energy dispersion in relation to the formation and temporal development of the CDPS in the flank of the magnetotail.

## 2 Instrumentation

We use ion and electron data from Fast Plasma Investigation (FPI) (Pollock et al., 2016) and magnetic field data from Fluxgate Magnetometer (FGM) (Russell et al., 2016) onboard MMS1, which is one of the four spacecraft in the MMS mission (Burch et al., 2016). The ion energy range of FPI for the event studied in this paper is from a few eV to 30 keV, which fully covered the typical energy of low-energy (cold) ions in the plasma sheet. Since burst-mode data were unavailable for the period of the current study, we use the fast survey-mode plasma data with a resolution of 4.5 s, which has no impact on the results presented in this paper. The four spacecraft were positioned at a distance of less than 20 km from each other, which is less than the ion kinetic scale. (The gyroradius of a 0.1-keV proton is  $\sim 70$  km in a 20-nT magnetic field.) During the events, all four spacecraft observed almost identical ion signatures at the resolution of 4.5 s, and thus we use only MMS1 data in this study. The solar wind data from the Advanced Composition Explorer (ACE) (Stone et al., 1998) and Wind spacecraft (Acuña et al., 1995) are referred to. The geocentric solar magnetospheric (GSM) coordinate system is used throughout.

## 3 Observations

Figure 1 presents an overview of MMS1 observations in the duskside magnetotail from 00:00 to 08:00 UT on 4 August 2017. For the first two hours, MMS1 remained in the lobe/mantle region in the northern hemisphere, which is characterised by a large  $B_x$  (Fig. 1a) and tailward plasma flows (Fig. 1f). CDPS observations continued for several hours between  $\sim 02:00$  and  $\sim 07:00$  UT. The omnidirectional ion energy-time (E-t) spectrogram illustrates the coexistence of high- and low-energy components (Fig. 1b), which is characteristic of the CDPS on the duskside under the northward IMF (Hasegawa et al., 2003; Nishino, Fujimoto, Ueno, Maezawa, et al., 2007; Wing et al., 2005). As discussed in the previous studies, the high-energy component is most likely of magnetospheric origin, while the low-energy component is thought to be recently supplied from the solar wind across the magnetopause. A recent simulation study by Sorathia et al. (2019) showed that the high-energy ions on the duskside include solar wind ions that enter through the cusps and become energized as they move along the dawn flank and cross the magnetotail from dawn to dusk, and that the low-energy ions on the duskside are those locally transported across the tail-flank magnetopause. The electron E-t spectrogram (Fig. 1c) reveals that low-energy electrons ( $< 1$  keV) were the main component of the CDPS. The solar wind conditions and the characteristics of the CDPS from 02:00 to 07:00 UT will be examined in the following.

The ion density and temperature in the CDPS were  $\sim 4\text{--}6\text{ cm}^{-3}$  and 0.4–0.7 keV, respectively (Fig. 1d and e). The parallel ion temperature is higher than the perpendicular ion temperature, which is consistent with previous statistical results (Nishino, Fujimoto, Ueno, Maezawa, et al., 2007). The plasma beta ( $\beta$ , the ratio of thermal pressure to magnetic pressure) in the CDPS was mainly between 1 and 10, which is characteristic of the



central plasma sheet. The bulk speed of the ion flows in the CDPS was very low (typically, below 50 km/s), which is consistent with the previous statistical results for geomagnetically quiet periods (e.g., Angelopoulos et al., 1993).

Solar wind data from ACE (Fig. 2a–e) and Wind (Fig. 2f–j) illustrate that the CDPS in the dusk magnetotail formed during a prolonged northward IMF. After 21:00 UT on 3 August 2017, the IMF pointed weakly northward, and then it turned strongly northward at around 01:00 UT on 4 August 2017 as both  $B_X$  and  $B_Y$  decreased. The IMF strength for the northward IMF period was higher than 10 nT. As the solar wind density data from ACE are available only for limited periods, we also use the data from Wind. The ACE and Wind spacecraft locations at 01:00 UT (which roughly corresponds to 02:00 UT at the Earth’s magnetosphere when the solar wind convection is considered) were  $(226, -21, -3)R_E$  and  $(234, 98, -14)R_E$  in the GSM coordinate system, respectively, where the Earth’s radius ( $R_E$ ) is defined as 6,378 km. The trends of the prolonged northward IMF and high-density solar wind plasma were observed at both the ACE and Wind locations. When MMS1 observed the CDPS in the magnetotail, the solar wind speed and density at ACE were  $\sim 400$  km/s and  $20\text{--}40\text{ cm}^{-3}$ , respectively. The solar wind conditions prior to the CDPS observations were steady near these values. The solar wind dynamic pressure was as high as 6–12 nPa, and the large temporal variation was attributed to the density fluctuations. The solar wind flow had relatively large azimuthal and latitudinal velocity components; a negative  $V_Y$  of  $\sim -60$  km/s until  $\sim 05:45$  UT and a positive  $V_Z$  of  $\sim 60$  km/s after  $\sim 04:20$  UT were detected. From 05:00 UT to 12:00 UT the solar wind speed gradually increased to become higher than  $\sim 600$  km/s. The increase in solar wind speed, density pile up, and tangential flow deflections all indicate the passage of a corotating interaction region.

At around 01:58 UT when MMS1 was located at  $(-22.6, 9.6, 4.3)R_E$  in the GSM coordinate system, the spacecraft moved from the northern lobe/mantle region to the stagnant CDPS region. Now we examine the ion E-t spectrograms in the directions parallel ( $0^\circ\text{--}30^\circ$ ), perpendicular ( $75^\circ\text{--}105^\circ$ ), and anti-parallel ( $150^\circ\text{--}180^\circ$ ) to the magnetic field (Fig. 3b–d). Throughout the period of the CDPS, both the parallel and anti-parallel fluxes in the low-energy range ( $< 3$  keV) were higher than the perpendicular flux. This observation is consistent with Nishino et al.’s (2007a) report of parallel anisotropy of low-energy ions in the duskside CDPS under the strongly northward IMF.

In addition, we have found energy dispersions of low-energy ions in both the parallel and anti-parallel directions (indicated by black arrows in Fig. 3b and d) that typically started at 1–2 keV and ended at 0.1–0.3 keV. These energy-dispersed ions were detected on the closed field lines, which is evidenced by bi-directional distributions of the low-energy electrons (Fig. 3i and j). The path length of these energy-dispersed ions from the acceleration source to the observing location can be estimated by assuming the time-of-flight (TOF) effect (e.g., Kazama & Mukai, 2003). From the start of the CDPS observation (at 01:57 UT) until 02:30 UT, the typical duration of the energy dispersion in the parallel direction was  $\sim 3$  min (at 01:58, 02:18, 02:22, 02:23, and 02:27 UT). In the anti-parallel direction, faint energy dispersions with longer durations ( $\sim 15$  min) were observed at around 02:17 UT and 02:27 UT. This signature may demonstrate that these ions were injected from the magnetotail plasma sheet toward the lower altitude region and came back toward the spacecraft by the mirror reflection. However, because the magnetic field direction changed within on a shorter timescale than the dispersion, we refrain from performing further analysis for this event.

We focus on the energy-dispersion event in the parallel direction between 02:23 and 02:26 UT (indicated by the thick arrow in Fig. 3b), when the dispersion signature was most obvious. As in previous studies (see Fig. 3 in Kazama and Mukai (2003) and Fig. 6 in Varsani et al. (2017)), we plot spectrograms of the reciprocal speed ( $V^{-1}$ ) of the ions with respect to time (Fig. 4e and f). The reciprocal speed linearly increased from 02:23 to 02:26 UT, which is attributed to the TOF effect of the injected ions. By extrapolating the

upper cutoff of the  $V^{-1}$ - $t$  slope backward in time, the time of the injection is estimated to be around 02:22:45 UT. The path length ( $L$ ) from the injection point to the spacecraft location is estimated as follows:

$$L = \frac{\Delta t}{\Delta(V^{-1})} = \frac{105 [\text{s}]}{0.005 [\text{km}^{-1}\text{s}]} = 3.3 R_E, \quad (1)$$

where  $0.005 \text{ km}^{-1}\text{s}$  was used as the upper cutoff of  $V^{-1}$  at 02:24:30 UT and 105 s was used as the traveling time, although the estimation errors are relatively large.

We further investigate the ion distribution function during the energy-dispersion event by making a two-dimensional slice in the plane including the local magnetic field direction. When drawing the slice, the bulk velocity perpendicular to the local magnetic field was subtracted in the velocity space. A slice in the middle of the event between 02:24:29 and 02:24:34 UT reveals a cold ion beam parallel to the magnetic field (Fig. 5). The beam had a peak around 270 km/s with a lower energy cutoff at around 180 km/s at which the energy flux was roughly  $1/e$  of the peak flux. The pitch angles of the beam ions were concentrated within  $30^\circ$ , with a broadened distribution up to  $45^\circ$ . The traveling time and path length from the injection point to the spacecraft location were estimated by a method described in Burch et al. (1982) that uses observed pitch-angle distributions and a geomagnetic field model. We compare the observed lower cutoff velocity of the energy flux with the theoretically calculated velocity, by modifying several injection points and traveling times, and adopting the T96 model (Tsyganenko & Stern, 1996) as the geomagnetic field. The black rectangles in Fig. 5 denote the lower cutoff estimated from the Burch's method under assumptions of a traveling time of 110 s and a path length of  $3.3 R_E$ , for the pitch angles every  $5^\circ$  between  $0^\circ$  and  $45^\circ$ . Although this method was unable to generate exact traveling times and path lengths for this event, the estimated values correspond with the observed lower cutoff velocity and thus are consistent with those obtained from the  $V^{-1}$ - $t$  spectrograms.

We use the T96 model to trace the magnetic field line to both the northern and southern polar regions. At 02:30 UT when MMS1 remained in the northern plasma sheet with a dominant positive  $B_X$ , the magnetic field line traced from the spacecraft's location toward the southern ionosphere crossed the neutral sheet  $\sim 10 R_E$  tailward of the spacecraft (Fig. 6). It is plausible that the ion beams in the parallel (earthward) direction emanated directly from the source, while the anti-parallel ion beams were reflected at lower altitudes in the northern hemisphere and returned to the magnetotail. The interval of the dispersive signatures in the parallel direction was roughly several minutes, and short dispersions in the parallel direction were more frequently detected than longer faint dispersions in the anti-parallel direction. This difference in detection frequencies could indicate a dependence on distance from the acceleration source.

We performed a global magnetohydrodynamic (MHD) simulation using the SWMF/BATS-R-US code with the Rice Convection Model (Tóth et al., 2005, 2012) to roughly estimate the relative position of the MMS1 spacecraft and the magnetopause on the duskside. We used the OMNI solar wind data as upstream conditions, except that the  $B_X$  component was fixed to be 3 nT through the simulation. Figure 7 presents the magnitude of the current density and the plasma density at 02:20 UT in the  $Z=4.2 R_E$  plane where the MMS1 spacecraft was located. Since the solar wind had a high dynamic pressure ( $\sim 10 \text{ nPa}$ ) and a significant dusk-to-dawn velocity component ( $\sim -60 \text{ km/s}$ ) (See Fig. 2), the magnetotail was strongly compressed and entirely shifted downward, and thus the MMS1 spacecraft at  $(-22.6, 9.6, 4.2) R_E$  was much closer to the dusk magnetopause than usual. This situation suggests that the injection source was not so far from the dusk-tail magnetopause, where the presence of well-developed vortices by the Kelvin-Helmholtz instability are expected under strongly northward IMF (Hasegawa et al., 2006).

We next examine the CDPS that was continuously observed a few hours after the strongly northward IMF came to the Earth's magnetosphere. Between 04:00–06:00 UT,

MMS1 remained in the CDPS where longer energy dispersions were observed in both the parallel and anti-parallel directions (Fig. 8). The ions signatures were similar to those in the preceding period, while  $B_Z$  dominated the magnetic field. The magnetic field strength and ion density in the CDPS were about 20 nT and  $5 \text{ cm}^{-3}$ , respectively, which gave a local Alfvén speed of  $\sim 180 \text{ km/s}$ .

We then focus on the energy dispersion event in the anti-parallel direction between 04:30 and 04:44 UT (Fig. 9). As in the previous event, a linear increase was revealed in the reciprocal speed of the energy-dispersed ions. By extrapolating the slope of the linear increase, we estimated that an ion injection event occurred at around 04:20 UT. Using the inclination of the slope, and the path length ( $L$ ) was estimated to be  $54 R_E$  as follows:

$$L = \frac{\Delta t}{\Delta(V^{-1})} = \frac{1200 [\text{s}]}{0.0035 [\text{km}^{-1} \text{s}]} = 54 R_E . \quad (2)$$

The estimated path length indicates that the energy-dispersed ions were previously mirror reflected at lower altitudes.

Fig. 10a and b show two-dimensional slices of the ion distribution functions at 04:35:20 UT and 04:40:20 UT (also denoted by the dashed lines in Fig. 9). The bulk velocity perpendicular to the local magnetic field was subtracted from the original data. We focus on an observed ion beam in the anti-parallel direction corresponding to the energy dispersion in the E-t spectrogram. At 04:35:20 UT, the energy flux of this beam component had a peak around 490 km/s with an elongated shape in the perpendicular direction. The pitch angle of the ion beam ranged between  $180^\circ$  and  $\sim 150^\circ$  with a broadened distribution in a crescent-like form. We calculated lower cutoff velocities using the Burch's method for several combinations of injection points and traveling durations to identify those with a good fit with the observed distribution functions. The estimated values are the injection point of  $5 R_E$  tailward of the MMS1 spacecraft (Fig. 10c) and the injection event at 04:19:20 UT (i.e., a traveling time of 960 s). The rectangles in Fig. 10a denotes the cutoff velocities calculated for pitch angles at increments of  $5^\circ$  between  $175^\circ$  and  $135^\circ$  under the assumption of an injection point of  $5 R_E$  tailward of MMS1 along the magnetic field line and the injection event at 04:19:20 UT.

Five minutes later at 04:40:20 UT, there was a decrease in both peak and cutoff speeds to 340 km/s and 280 km/s, respectively. A combination of the same injection point as above and a traveling time of 1260 s gave cutoff velocities that well fitted the observations (Fig. 10b). This traveling time corresponds to the injection event at 04:19:20 UT, which roughly matches the event time estimated from the  $V^{-1}$ - $t$  slope. The path length of the mirror reflected ions (i.e., from the injection source via the mirror point to the observed location) is strongly contingent on the pitch angle. A calculation of path length using the T96 model for a pitch angle of  $175^\circ$  at the MMS1 spacecraft gives  $54 R_E$ , which is consistent with the estimation by the  $V^{-1}$ - $t$  slope. These ions were mirror reflected at  $(-0.72, 0.88, 2.6) R_E$  in GSM where the magnetic field strength was 2510 nT. On the other hand, the path length for a pitch angle of  $150^\circ$  was calculated to be  $38 R_E$ : the location and the magnetic field strength of the mirror point were  $(-6.7, 4.7, 5.2) R_E$  in GSM and 76 nT, respectively. The path length in this estimation is dependent solely on the location of the mirror point, as the same injection point is assumed for all pitch angles. We assumed that the pitch angle is precisely equal to  $180^\circ$  when the path length from the  $V^{-1}$ - $t$  slope in the anti-parallel direction was estimated. No contradiction exists between the shorter path length estimated for a pitch angle of  $150^\circ$  and the entire scenario of the injection and mirror reflection.

We surveyed energy dispersion events in the CDPS between 02:00 and 07:00 UT and identified 12 events in the parallel direction and 9 events in the anti-parallel direction (Table 1 and Fig. 11). We adopted only the events with the clearly defined upper edge of the linearly increasing  $V^{-1}$ - $t$  slope and rejected events with ambiguous slopes and those without a linear increase. We also excluded cases where the magnetic field changed sig-

nificantly during the energy-dispersion events. During the 5 hours of the CDPS observation, MMS1 stayed mainly in the northern plasma sheet where  $B_X$  was positive (directed earthward), and most energy-dispersion events were detected in the northern plasma sheet, except for a few events during excursions to the southern plasma sheet. Most of the parallel beams had short path lengths ( $<10 R_E$ ), which means direct injection from the source to the spacecraft location without accessing lower altitudes. In contrast, the anti-parallel beams frequently had longer path lengths ( $>30 R_E$ ), which means that these ions were magnetically reflected at lower altitudes. One anti-parallel beam event with a short path length was observed in the southern plasma sheet, which shows that the beam came from the injection source directly to the spacecraft location. In the anti-parallel beam event at 05:40 UT, ion energy went down from 3 keV to  $\sim 0.3$  keV. This fact suggests that some fraction of the high-energy ions in the cold-dense plasma sheet originated from the low-energy component that came from the solar wind recently.

After 06:00 UT, no apparent energy dispersions were recognised in parallel and anti-parallel directions, despite the spacecraft still staying in the cold-dense plasma sheet. The cease of energy-dispersion events may be related to the end of the prolonged strongly northward IMF at around 06:00 UT (around 05:00 UT at ACE location). In addition, a decrease of the dusk-to-dawn component of the solar wind flow may relocate the magnetotail, decreasing the detection probability of energy dispersions at the MMS1 location, if ion injections have occurred near the magnetopause boundary.

It is likely that the energy dispersion of low-energy ions generally occurs in the well-developed CDPS several hours after the start of the strongly northward IMF. The CDPS dominated by  $B_Z$  is consistent with the plasma sheet thickening and an increase in the total plasma content (Fuselier et al., 2015; Nishino et al., 2002). The prolonged presence of a large  $B_Z$  in the CDPS under the strongly northward IMF suggests that the magnetic field lines of the near-Earth magnetotail shifted from a tail-like shape to a less-stretched shape, which was reported in previous research by Petrukovich et al. (2003). If the large  $B_Z$  of the CDPS in this event is the result of the plasma sheet thickening under the strongly northward IMF, it is interesting to note that plasma sheet thickening and thus increased magnetotail plasma content are simultaneously observed with low-energy ion transport by injection.

For most of the time, the bulk ion speed in the CDPS was as low as  $\sim 50$  km/s, which is consistent with previous statistical results (e.g., Angelopoulos et al., 1993) and event studies (e.g., Fujimoto et al., 1998). We note that even when energy dispersion occurs, both the parallel and perpendicular velocities are low. In the velocity moment calculation, since the parallel and anti-parallel components negate each other, the low parallel velocity does not contradict the observed ion transport in the field-aligned direction.

## 4 Summary and Discussion

We identified energy-dispersed low-energy ions in the CDPS in the duskside magnetotail under the strongly northward IMF and analyzed injection points in two ways, that is, by assuming the TOF effect and by using information of pitch angle dispersions. During the first event, the energy-dispersed ions in the direction parallel to the magnetic field were deemed to have originated from the tail flank plasma sheet several  $R_E$  tailward of the MMS1 spacecraft's location. During the second event, a longer duration of the ion energy dispersion in the anti-parallel direction was evident, which indicates that these ions once traveled along the magnetic field toward the ionosphere and were mirror reflected at a low altitude back to the magnetotail plasma sheet.

The energy-dispersed ions in the field-aligned directions are not inconsistent with the stagnant plasma flows in the CDPS under the northward IMF. This is because the ion velocities in the parallel and anti-parallel directions were negated and thus did not exist in

**Table 1.** The list of the parallel and anti-parallel energy-dispersion events between 02:00–07:00 UT. Most events occurred in the northern plasma sheet unless otherwise noted.

(a) Events of the parallel beams (northward-going beams).

Time (UT)	Path length ( $R_E$ )	Note
02:16	7.8	
02:22	1.6	
02:23	3.3	Studied in the main text.
02:26	6.4	
03:18	38	Southern plasma sheet
03:37	2.9	
03:48	4.2	
03:54	4.5	
04:08	5.3	
04:15	27	
04:55	17	
05:18	1.8	

(b) Events of the anti-parallel beams (southward-going beams).

Time (UT)	Path length ( $R_E$ )	Note
02:20	32	
02:28	40	
03:19	12	Southern plasma sheet, High energy (from 3 keV to 1 keV)
03:33	3.4	
04:08	65	Southern plasma sheet
04:14	38	
04:20	54	Studied in the main text
05:08	18	
05:40	38	High energy (from 3 keV to 0.3 keV)

the bulk velocity, i.e., the low bulk velocity obtained from the moment calculation did not necessarily indicate the dominance of diffusive plasma transport.

The observed energy dispersions mean that some acceleration mechanisms would work in the tail flank region. Possible candidates for the acceleration mechanism of the energy-dispersed ions are (1) magnetic reconnection in well-developed Kelvin-Helmholtz vortices (e.g., Nakamura et al., 2017; Nishino, Fujimoto, Ueno, Mukai, & Saito, 2007; Takagi et al., 2006), (2) tension force of the closed magnetic field lines (Fujimoto et al., 1996), and (3) additional mechanisms including small magnetic reconnection in the turbulent plasma sheet (Borovsky & Funsten, 2003).

During the events reported in this study, the magnetopause under the strongly northward IMF was likely to be Kelvin-Helmholtz unstable to generate vortical structures flowing tailward (e.g., Kavosi & Raeder, 2015). As shown in the global MHD simulation, the MMS1 spacecraft was likely located not so far from the dusk-tail magnetopause due to the entire dawnward shift of the highly compressed magnetotail, which suggests that the injection accelerating low-energy ions may be related to the magnetopause processes such as Kelvin-Helmholtz vortices. The intervals of energy dispersive signatures were a few to several minutes, which is similar to the period of the Kelvin-Helmholtz vortices in the magnetotail flanks (e.g., Nishino et al., 2011). In previous studies, ion beams observed in the LLBL under the northward IMF have been interpreted in the context of Kelvin-Helmholtz instability (Nishino, Fujimoto, Ueno, Mukai, & Saito, 2007; Taylor & Lavraud, 2008). Stenuit et al. (2001, 2002) reported the detection of energy-dispersed ions in the LLBL at the low-altitude region under the northward IMF, and suggested that Kelvin-Helmholtz instability at the tail magnetopause is related to the generation of energy-dispersed ions. The speed of the ion beams in the LLBL that were possibly accelerated inside the Kelvin-Helmholtz vortices is estimated to be in the order of the reconnection Alfvén speed (e.g., Ma et al., 2017). The LLBL was not detected directly in this study, but the local Alfvén speed in the CDPS was around 180 km/s (for a density of  $5 \text{ cm}^{-3}$  and a magnetic field strength of 20 nT), which is below the observed maximum speed of the energy-dispersed ions (typically, 400–500 km/s). However, if magnetic reconnection occurs in the lower density region closer to the plasma sheet boundary layer, the higher Alfvén speed may explain the maximum speed of the ion beams.

The plasma flow during the energy-dispersion events was relatively stagnant ( $<50 \text{ km/s}$ ) (See Figs. 3g and 8g), which is consistent with previous studies of the CDPS. We note that the speed of observed parallel and anti-parallel ion beams was much higher than the bulk ion speed, and that the perpendicular velocity did not show fast earthward flow that can be expected for large-scale magnetic reconnection. The fact that no fast perpendicular flow was observed suggests that magnetic reconnection accelerating the observed ions was transient and not spatially extended and did not affect the global configuration of the Earth's magnetic field lines.

A scenario of the tension force of the closed field lines in the LLBL or in the CDPS adjacent to the LLBL is considered. The closed field lines in the LLBL/CDPS are stretched tailward by viscous interactions with the magnetosheath plasma, and finally return toward the Earth by the magnetic tension force (Fujimoto et al., 1996). This process may accelerate the ions toward the Earth and would be evidenced by the occurrence of fast bulk flows. However, because no fast earthward flows were detected by MMS during the events in this study, it is unlikely that magnetic tension force effectively generates the observed energy-dispersed structures.

Considering the origins of the cold-dense plasma, although double-lobe reconnection is the most plausible mechanism for capturing the magnetosheath plasma into the Earth's magnetosphere, formation of the lobe/mantle region is also a potential candidate for the entry process. MMS1 data before 01:58 UT confirm the entry of large amounts of cold ions into the magnetotail via the lobe/mantle region during the northward IMF with an



enhanced IMF  $B_Y$ . It is possible that the low-energy ions from the lobe/mantle region are the partial source of the energy-dispersed ions detected in the plasma sheet after 01:58 UT, since the detection of the CDPS by MMS1 started in the outer plasma sheet close to the northern lobe, as indicated by the large  $B_X$  component.

We discuss the possible relationship between energy-dispersed ions and the magnetosphere-ionosphere coupling under the northward IMF. Stenuit et al. (2002) proposed a connection between the energy-dispersed ions at a low altitude and the Kelvin-Helmholtz instability at the tail magnetopause and demonstrated outflows of ionospheric oxygen ions under the northward IMF. Wang et al. (2019) examined the CDPS events observed by MMS in the magnetotail and DMSP-F18 in a low-altitude orbit and found increases in the density of oxygen ions ( $O^+$ ) of ionospheric origin at both locations under the northward IMF. Their research revealed signatures of kinetic Alfvén waves that are capable of accelerating electrons in the field-aligned direction, and they discussed that observed electrons injected from the magnetosphere into the ionosphere playing a key role in the outflow of oxygen ions from the ionosphere to the CDPS. The events in the current study was also analyzed by Wang et al. (2019), i.e., the energy-dispersed ions in the CDPS coincided with the increase in the oxygen ions from the ionosphere. It is worth noting that both kinetic Alfvén waves and ion injection can be caused by magnetic reconnection in the Kelvin-Helmholtz vortices. The major carrier of field-aligned current may be electrons accelerated by kinetic Alfvén waves, which is consistent with the present study's observation of the low ion bulk speed in the parallel direction. Yokoyama et al.'s (2020) recent observational study analyzed low-altitude satellite data and proposed a generation mechanism of mesoscale field-aligned currents in the LLBL on the duskside during northward IMF periods. Their observation of the 630-nm auroral emission in the upward field-aligned current regions indicates that the major carrier of the field-aligned currents under the northward IMF is electrons precipitating into the ionosphere. However, because the present study was conducted for the stagnant CDPS and not for the LLBL with tailward flows, further investigations are required.

The energy dispersion of the low-energy ions in the current study occurred under a condition of high-density solar wind. Although the effect of solar wind density on the occurrence of the energy dispersion of the low-energy ions remains unclear, other CDPS events with ion energy dispersion under conditions of the strongly northward IMF and moderate solar wind density (data not shown here) have been identified. Therefore, the authors consider that the field-aligned transport of low-energy ions in the near-Earth plasma sheet generally occurs under the strongly northward IMF. However, further study is required into detailed mechanisms of ion acceleration under the strongly northward IMF and plasma transport under the weakly northward IMF. Further research will also explore the low-energy ion signatures in the CDPS in the dawn magnetotail as well as in the dawn LLBL under the strongly northward IMF.

#### Data Availability Statement

MMS data are available from <https://lasp.colorado.edu/mms/sdc/public/>. Solar wind data from ACE and Wind were provided by NASA's CDAWeb (<https://cdaweb.gsfc.nasa.gov/>). Data analysis was performed using SPEDAS V3.1 (see Angelopoulos et al. (2019) in detail).

The global MHD simulation of the Earth's magnetosphere was carried out using the Space Weather Modeling Framework (SWMF) and The Block Adaptive Tree Solar wind Roe-type Upwind Scheme (BATS-R-US) tools developed at the University of Michigan's Center for Space Environment Modeling (CSEM). The modelling tools described in this publication are available online through the University of Michigan for download and are available for use at the Community Coordinated Modeling Center (CCMC) at Goddard Space Flight Center. All simulation data used in this study have been provided by

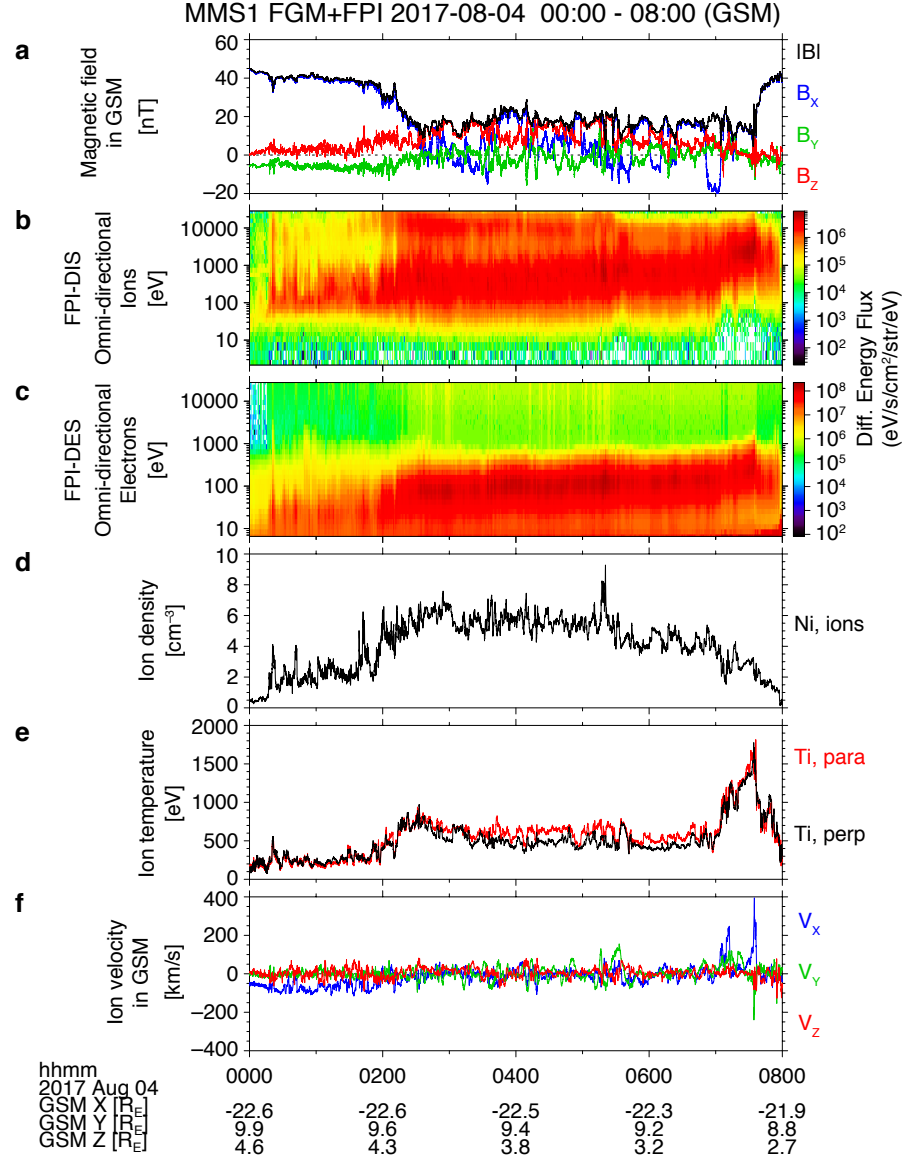


**Figure 1.** An overview of MMS1 observations between 00:00–08:00 UT on August 4, 2017. From the top: (a) magnetic field, (b) omnidirectional ion energy-time spectrogram, (c) omnidirectional electron energy-time spectrogram, (d) ion density, (e) parallel (red) and perpendicular (black) ion temperatures, and (f) ion velocity. The energy-time spectrograms are shown in the unit of differential energy flux.



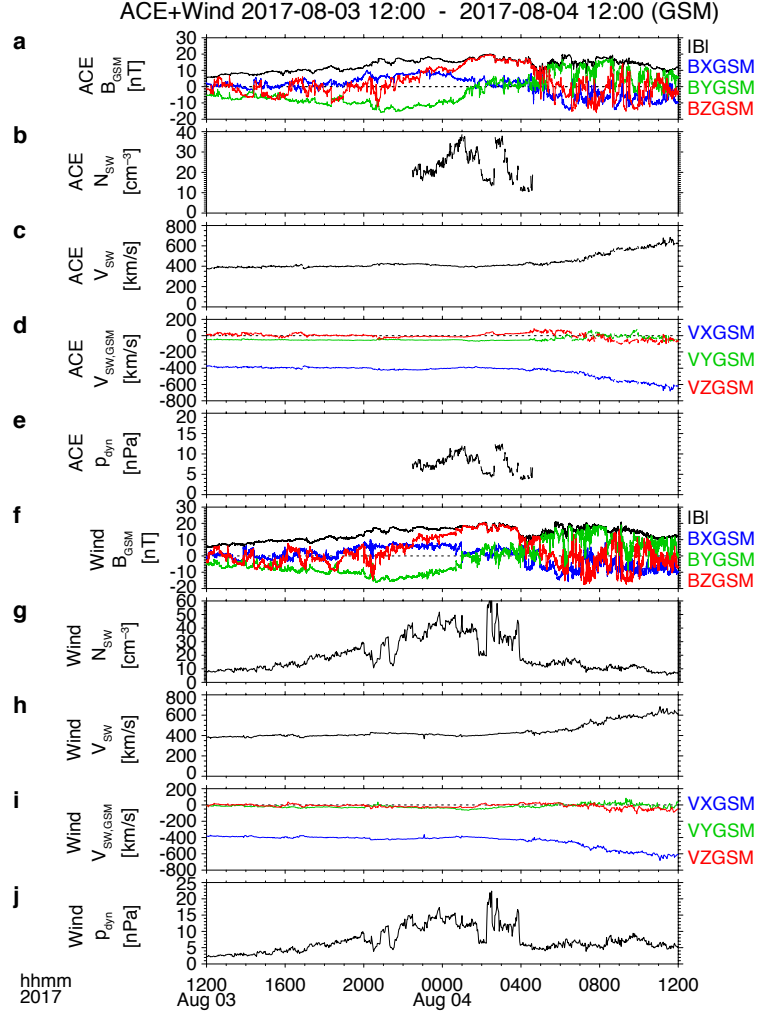


**Figure 2.** Solar wind data from ACE and Wind for 24 hours from 12:00 UT on August 3, 2017. From the top, (a) magnetic field, (b) ion density, (c) ion bulk speed, (d) ion flow vector, and (e) dynamic pressure from ACE. (f-j) Data from Wind are plotted in the same format as the ACE data.

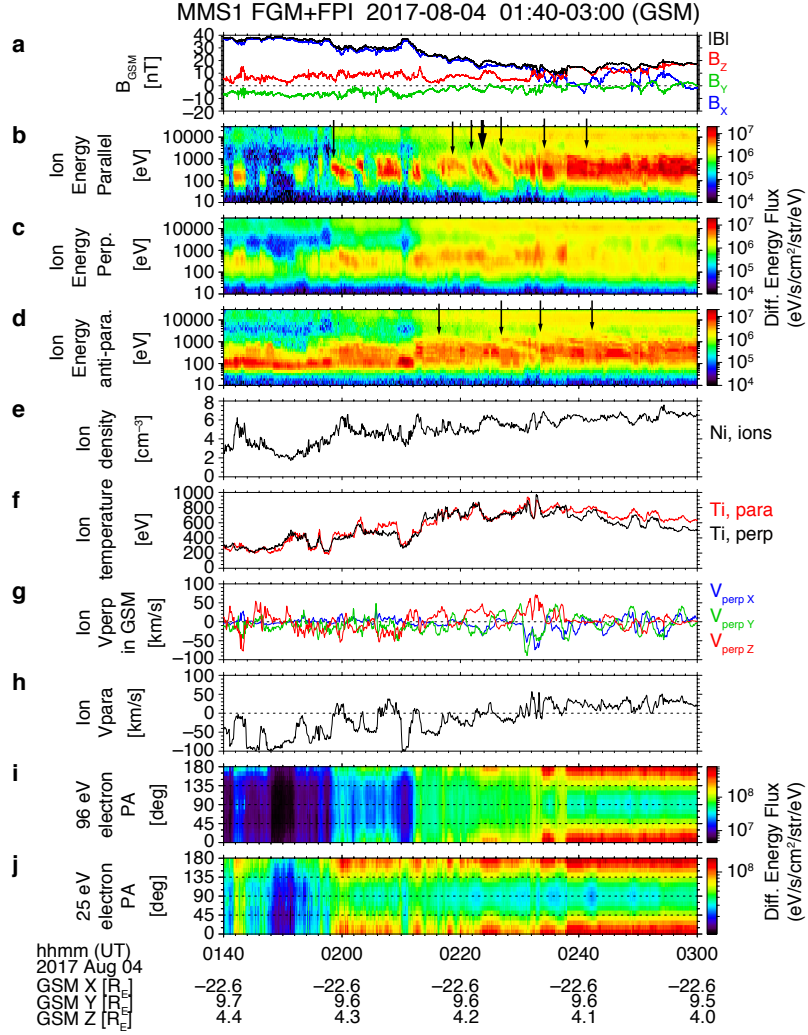


**Figure 3.** MMS1 observations between 01:40–03:00 UT on August 4, 2017. (a) Magnetic field, (b-d) ion energy-time spectrograms parallel, perpendicular, and anti-parallel to the magnetic field, (e) ion density, (f) ion parallel and perpendicular temperatures, (g) bulk ion velocity in the direction perpendicular to the local magnetic field, (h) bulk ion velocity in the parallel direction, (i) 96-eV electron pitch-angle distribution and (j) 25-eV electron pitch-angle distribution. Each arrow in the ion energy-time spectrograms indicates the beginning of energy dispersion. The thick arrow corresponds to the dispersion event analysed in detail in the main text.

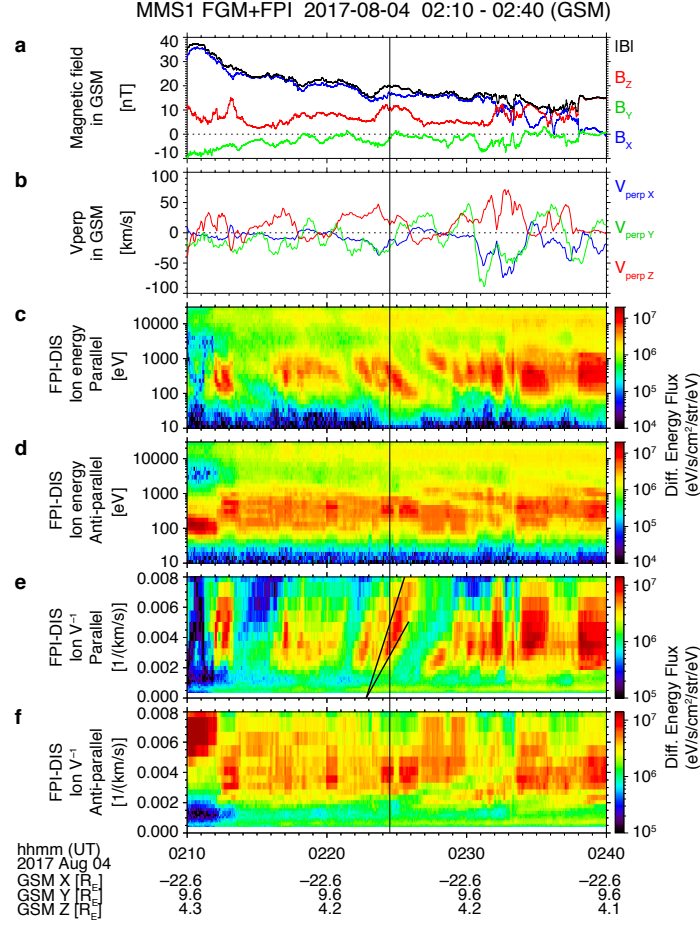


**Figure 4.** Energy-time spectrograms and reciprocal speed ( $V^{-1}$ )-time spectrograms between 02:10–02:40 UT. (a) Magnetic field, (b) bulk ion velocity perpendicular to the magnetic field, (c and d) ion E-t spectrograms parallel and anti-parallel to the magnetic field, (e and f) reciprocal speed-time spectrograms in parallel and anti-parallel directions. A vertical dashed line marks the time when a two-dimensional slice of ion distribution function in Fig. 5 was taken.

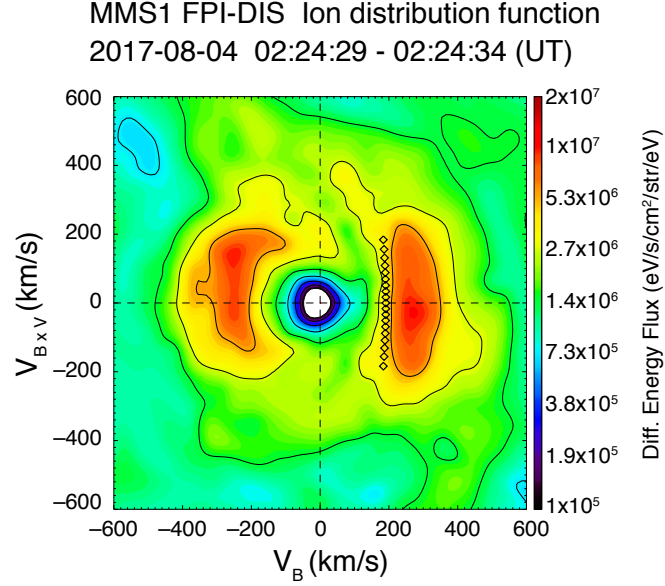


**Figure 5.** Two-dimensional slice of ion distribution function between 02:24:29–02:24:34 UT. The horizontal axis is the local magnetic field direction. The black rectangles show the lower cutoff of the distribution function of the ion beam for the pitch angles every  $5^\circ$  from  $0^\circ$  to  $45^\circ$  calculated using the Burch’s method (Burch et al., 1982).

2017-08-04 02:20 UT Magnetic field model (Tsyganenko 1996 in GSM)

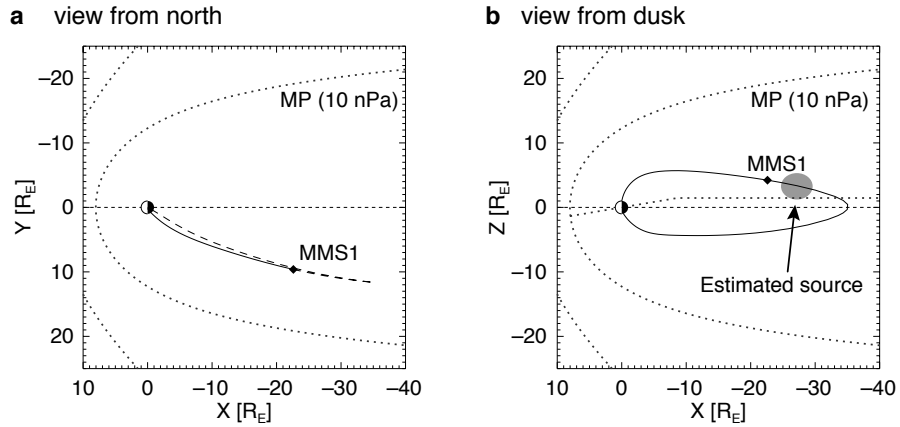


**Figure 6.** Traced magnetic field line at MMS1 using the T96 model at 02:20 UT. In the left panel, a solid (dotted) curve shows the magnetic field line traced from the MMS1 location toward the northern (southern) polar region. A dotted parabolic curve indicated by ‘MP’ is the modeled magnetopause location under a high solar wind dynamic pressure of 10 nPa (Shue et al., 1998). Please note that the effect of non-radial components of the solar wind flow is not included in the magnetopause model. The entire magnetotail in this event was shifted downward due to the significant dusk-to-dawn component of the solar wind flow, as shown in Fig. 7. A grey region illustrates a roughly estimated source of the energy-dispersed ions.

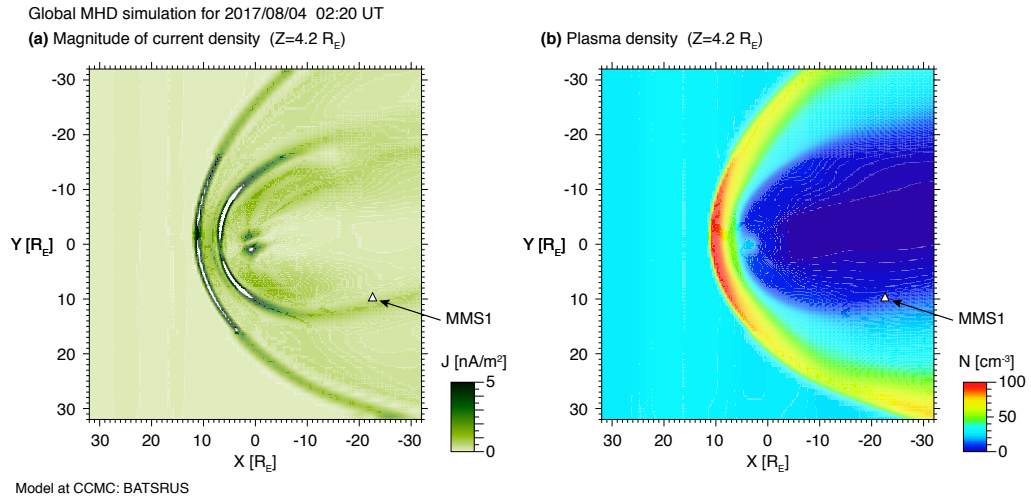


**Figure 7.** Results of a global MHD simulation using the SWMF/BATS-R-US code with Rice Convection Model (Tóth et al., 2005, 2012). (a) The magnitude of the current density and (b) the plasma density in the  $Z=4.2 R_E$  plane where MMS1 was located are presented in the linear color scale.

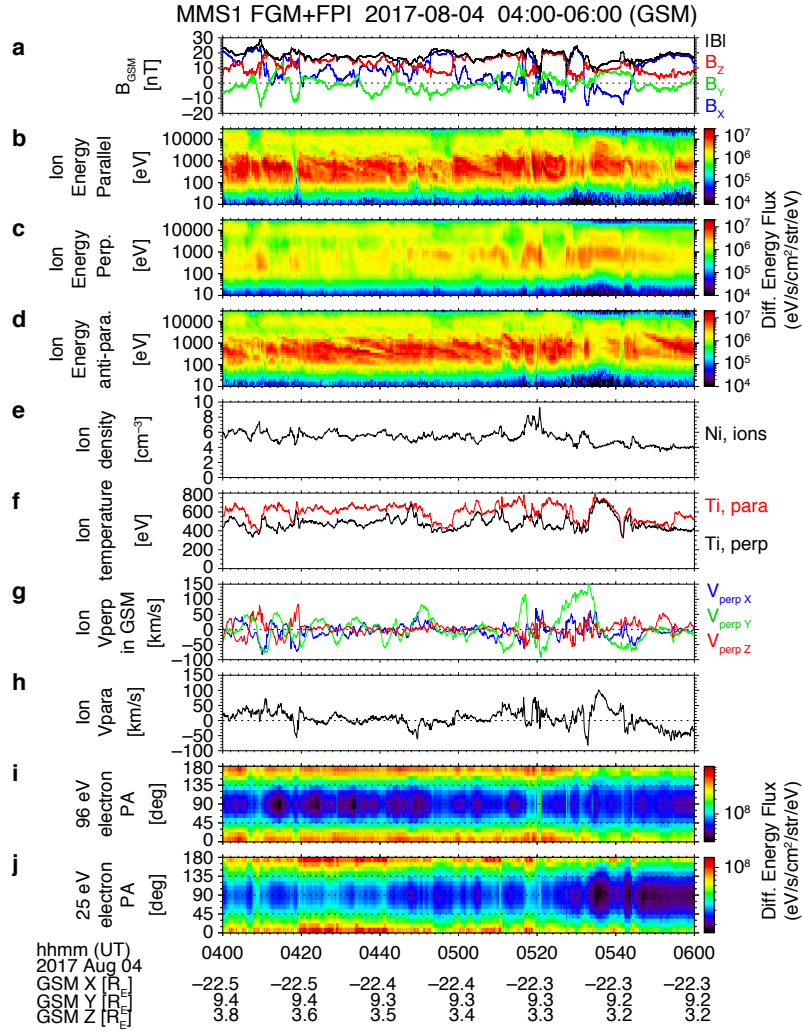


**Figure 8.** MMS1 observations between 04:00–06:00 UT on August 4, 2017 in the same format as Fig. 3.

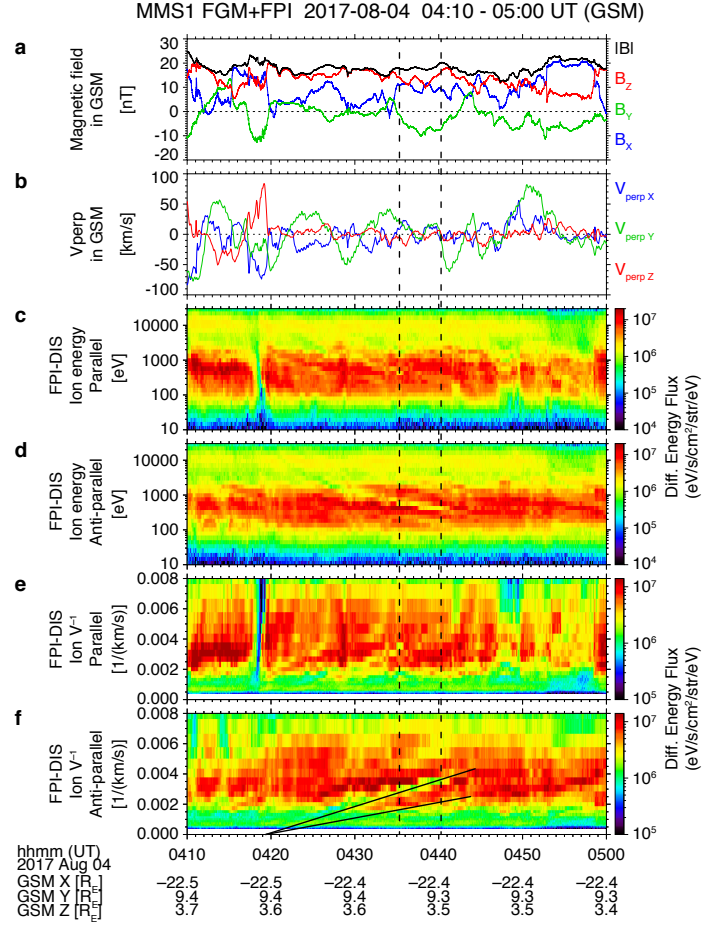
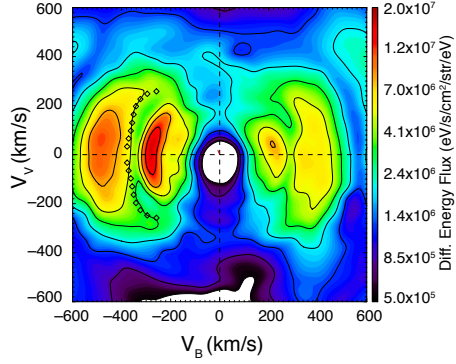


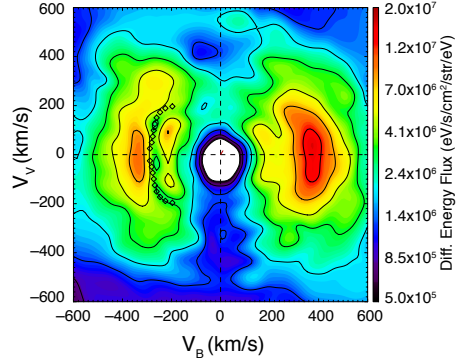
**Figure 9.** MMS1 data between 04:10–05:00 UT in the same format as Fig. 4. Two vertical lines correspond to the data presented in Fig. 10.

MMS1/FPI-DIS Ion distribution functions

(a) 04:35:17 – 04:35:22 (UT)



(b) 04:40:19 – 04:40:23 (UT)



(c) A schematic picture of mirror-reflected ion path (not in scale)

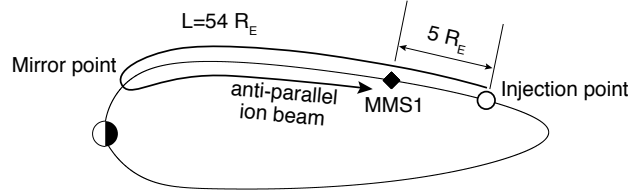


**Figure 10.** Two-dimensional slices of the ion distribution functions (a) between 04:35:17–04:35:22 UT and (b) between 04:40:19–04:40:23 UT. The black rectangles show the lower-energy cutoff of the distribution function of the ion beam for the pitch angles every  $5^\circ$  from  $175^\circ$  to  $135^\circ$  calculated using the Burch’s method (Burch et al., 1982). (c) A schematic picture of ion path from the estimated injection point to the MMS1 location via the mirror point at lower altitude. The path length ( $L=54 R_E$ ) estimated from the energy-dispersion analysis is presented, although the length depends on pitch angle of the particles (See main text).



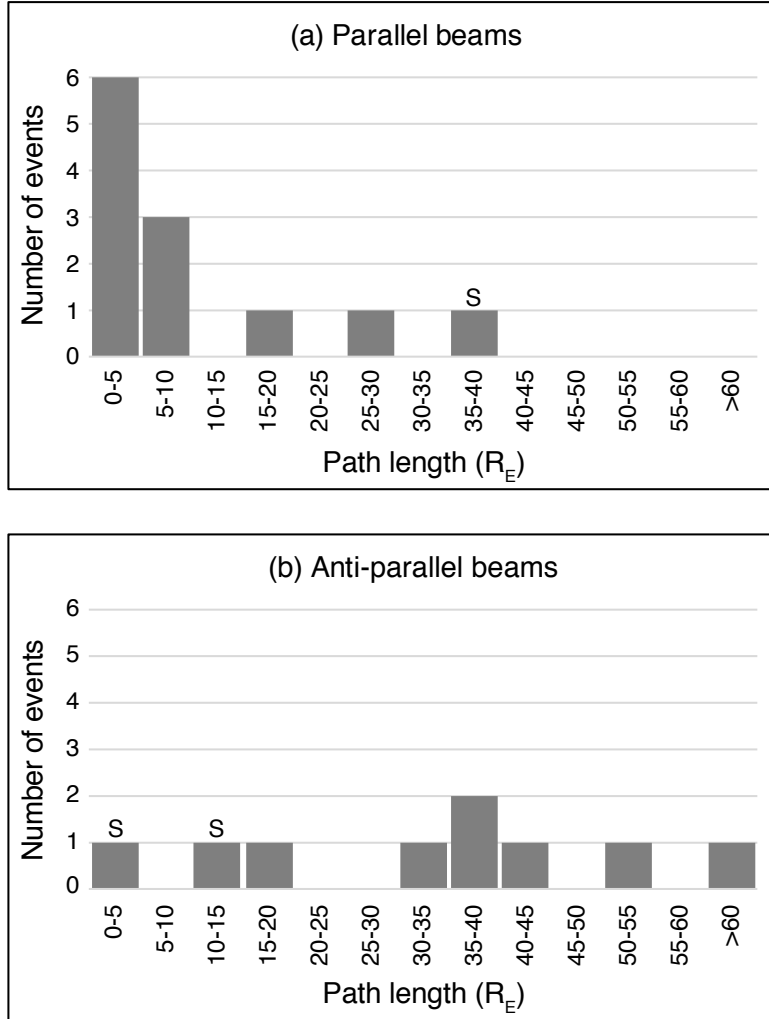


**Figure 11.** Histograms of energy-dispersion events in the parallel and anti-parallel directions between 02:00 and 07:00 UT. The symbol S in the histograms indicates that those events were observed in the southern plasma sheet.

the CCMC through their public Runs on Request system and are available at the following website.  
[https://ccmc.gsfc.nasa.gov/results/viewrun.php?domain=GM&runnumber=Masaki.Nishino.020120\\_1](https://ccmc.gsfc.nasa.gov/results/viewrun.php?domain=GM&runnumber=Masaki.Nishino.020120_1)

## Acknowledgments

The authors are grateful to the entire MMS team and instrument leads for data access and support. Craig J. Pollock, Thomas E. Moore, James L. Burch, Jean-Andre Sauvaud, William R. Paterson, John Dorelli, Daniel Gershman, Conrad Schiff, Levon Avanov, Benoit Lavraud, Michael Chandler and Victoria Coffey are acknowledged for providing instrumentation and data production/quality for the FPI instrument. The authors gratefully acknowledge the development team of the Space Physics Environment Data Analysis System (SPEDAS) software and thank the principal investigators of the ACE and Wind spacecraft for providing solar wind data through CDAWeb at NASA. Finally, Kazushi Asamura and Masaki Fujimoto are acknowledged for providing fruitful discussions.

This research was supported by the NASA MMS mission in association with NASA contract NNG04EB99C. Institut de Recherche en Astrophysique et Planétologie (IRAP) contributions to MMS FPI were supported by Centre National d'Études Spatiales (CNES) and Centre National de la Recherche Scientifique (CNRS). The work of MNN was supported by JSPS KAKENHI Grant Number 19K03947, and the work of TN at ISAS/JAXA was supported by MEXT/JSPS KAKENHI Grant Number 17H06140.

## References

- Acuña, M. H., Ogilvie, K. W., Baker, D. N., Curtis, S. A., Fairfield, D. H., & Mish, W. H. (1995). The Global Geospace Science Program and its investigations. *Space Science Reviews*, 71(1), 5–21. Retrieved from <https://doi.org/10.1007/BF00751323> doi: 10.1007/BF00751323
- Allen, R. C., Livi, S. A., Vines, S. K., & Goldstein, J. (2016). Magnetic latitude dependence of oxygen charge states in the global magnetosphere: Insights into solar wind-originating ion injection. *Journal of Geophysical Research: Space Physics*, 121(10), 9888–9912. Retrieved from <https://agupubs.onlinelibrary.wiley.com/doi/abs/10.1002/2016JA022925> doi: <https://doi.org/10.1002/2016JA022925>
- Angelopoulos, V., Cruce, P., Drozdov, A., Grimes, E. W., Hatzigeorgiu, N., King, D. A., ... Schroeder, P. (2019). *The Space Physics Environment Data Analysis System (SPEDAS)*. doi: 10.1007/s11214-018-0576-4
- Angelopoulos, V., Kennel, C. F., Coroniti, F. V., Pellat, R., Spence, H. E., Kivelson, M. G., ... Russell, C. T. (1993, aug). Characteristics of ion flow in the quiet state of the inner plasma sheet. *Geophysical Research Letters*, 20(16), 1711–1714. Retrieved from <http://doi.wiley.com/10.1029/93GL00847> doi: 10.1029/93GL00847
- Borovsky, J. E., & Funsten, H. O. (2003). MHD turbulence in the Earth's plasma sheet: Dynamics, dissipation, and driving. *Journal of Geophysical Research: Space Physics*. doi: 10.1029/2002JA009625
- Borovsky, J. E., Thomsen, M. F., & Elphic, R. C. (1998). The driving of the plasma sheet by the solar wind. *Journal of Geophysical Research: Space Physics*. doi: 10.1029/97ja02986
- Burch, J. L., Moore, T. E., Torbert, R. B., & Giles, B. L. (2016). *Magnetospheric Multiscale Overview and Science Objectives*. doi: 10.1007/s11214-015-0164-9
- Burch, J. L., Reiff, P. H., Heelis, R. A., Winningham, J. D., Hanson, W. B., Gurgiolo, C., ... Barfield, J. N. (1982). Plasma injection and transport in the mid-altitude polar cusp. *Geophysical Research Letters*. doi: 10.1029/GL009i009p00921
- Fairfield, D. H., Otto, A., Mukai, T., Kokubun, S., Lepping, R. P., Steinberg, J. T., ... Yamamoto, T. (2000). Geotail observations of the Kelvin-Helmholtz instability at the equatorial magnetotail boundary for parallel northward fields. *Journal of Geophysical Research: Space Physics*. doi: 10.1029/1999ja000316
- Fujimoto, M., Nishida, A., Mukai, T., Saito, Y., Yamamoto, T., & Kokubun, S. (1996). Plasma entry from the flanks of the near-Earth magnetotail: GEOTAIL observations in the dawnside LLBL and the plasma sheet. *Journal of Geomagnetism and Geoelectricity*. doi: 10.5636/jgg.48.711
- Fujimoto, M., Terasawa, T., Mukai, T., Saito, Y., Yamamoto, T., & Kokubun, S. (1998). Plasma entry from the flanks of the near-Earth magnetotail: Geotail observations. *Journal of Geophysical Research: Space Physics*. doi: 10.1029/97ja03340
- Fuselier, S. A., Dayeh, M. A., Livadiotis, G., McComas, D. J., Ogasawara, K., Valek, P., ... Petrinc, S. M. (2015). Imaging the development of the cold dense plasma sheet. *Geophysical Research Letters*. doi: 10.1002/2015GL065716
- Hasegawa, H., Fujimoto, M., Maezawa, K., Saito, Y., & Mukai, T. (2003). Geotail observations of the dayside outer boundary region: Interplanetary magnetic field control and dawn-dusk asymmetry. *Journal of Geophysical Research: Space Physics*. doi: 10.1029/2002JA009667
- Hasegawa, H., Fujimoto, M., Phan, T. D., Rème, H., Balogh, A., Dunlop, M. W., ... Tan-Dokoro, R. (2004). Transport of solar wind into Earth's magnetosphere through rolled-up Kelvin-Helmholtz vortices. *Nature*. doi: 10.1038/nature02799
- Hasegawa, H., Fujimoto, M., Takagi, K., Saito, Y., Mukai, T., & Rème, H. (2006). Single-spacecraft detection of rolled-up Kelvin-Helmholtz vortices at the flank magnetopause. *Journal of Geophysical Research: Space Physics*, 111(A9). Retrieved from <https://agupubs.onlinelibrary.wiley.com/doi/abs/10.1029/2006JA011728> doi: <https://doi.org/10.1029/2006JA011728>

- Kavosi, S., & Raeder, J. (2015). Ubiquity of Kelvin-Helmholtz waves at Earth's magnetopause. *Nature Communications*, 6(1), 7019. Retrieved from <https://doi.org/10.1038/ncomms8019> doi: 10.1038/ncomms8019
- Kazama, Y., & Mukai, T. (2003). Multiple energy-dispersed ion signatures in the near-Earth magnetotail: Geotail observation. *Geophysical Research Letters*. doi: 10.1029/2002GL016637
- Li, W., Raeder, J., Dorelli, J., Øieroset, M., & Phan, T. D. (2005). Plasma sheet formation during long period of northward IMF. *Geophysical Research Letters*. doi: 10.1029/2004GL021524
- Ma, X., Delamere, P., Otto, A., & Burkholder, B. (2017). Plasma transport driven by the three-dimensional Kelvin-Helmholtz instability. *Journal of Geophysical Research: Space Physics*. doi: 10.1002/2017JA024394
- Nagata, D., MacHida, S., Ohtani, S., Saito, Y., & Mukai, T. (2008). Solar wind control of plasma number density in the near-Earth plasma sheet: Three-dimensional structure. *Annales Geophysicae*. doi: 10.5194/angeo-26-4031-2008
- Nakamura, T. K., Hasegawa, H., Daughton, W., Eriksson, S., Li, W. Y., & Nakamura, R. (2017). Turbulent mass transfer caused by vortex induced reconnection in collisionless magnetospheric plasmas. *Nature Communications*. doi: 10.1038/s41467-017-01579-0
- Nishino, M. N., Fujimoto, M., Terasawa, T., Ueno, G., Maezawa, K., Mukai, T., & Saito, Y. (2007). Geotail observations of temperature anisotropy of the two-component protons in the dusk plasma sheet. *Annales Geophysicae*. doi: 10.5194/angeo-25-769-2007
- Nishino, M. N., Fujimoto, M., Ueno, G., Maezawa, K., Mukai, T., & Saito, Y. (2007). Geotail observations of two-component protons in the midnight plasma sheet. *Annales Geophysicae*. doi: 10.5194/angeo-25-2229-2007
- Nishino, M. N., Fujimoto, M., Ueno, G., Mukai, T., & Saito, Y. (2007). Origin of temperature anisotropies in the cold plasma sheet: Geotail observations around the Kelvin-Helmholtz vortices. *Annales Geophysicae*. doi: 10.5194/angeo-25-2069-2007
- Nishino, M. N., Hasegawa, H., Fujimoto, M., Saito, Y., Mukai, T., Dandouras, I., ... Schwartz, S. J. (2011). A case study of Kelvin-Helmholtz vortices on both flanks of the Earth's magnetotail. *Planetary and Space Science*. doi: 10.1016/j.pss.2010.03.011
- Nishino, M. N., Terasawa, T., & Hoshino, M. (2002). Increase of the tail plasma content during the northward interplanetary magnetic field intervals: Case studies. *Journal of Geophysical Research: Space Physics*. doi: 10.1029/2002JA009268
- Petrukovich, A. A., Baumjohann, W., Nakamura, R., Balogh, A., Mukai, T., Glassmeier, K. H., ... Klecker, B. (2003). Plasma sheet structure during strongly northward IMF. *Journal of Geophysical Research: Space Physics*. doi: 10.1029/2002JA009738
- Pollock, C., Moore, T., Jacques, A., Burch, J., Gliese, U., Saito, Y., ... Zeuch, M. (2016). *Fast Plasma Investigation for Magnetospheric Multiscale*. doi: 10.1007/s11214-016-0245-4
- Russell, C. T., Anderson, B. J., Baumjohann, W., Bromund, K. R., Dearborn, D., Fischer, D., ... Richter, I. (2016). *The Magnetospheric Multiscale Magnetometers*. doi: 10.1007/s11214-014-0057-3
- Shue, J.-H., Song, P., Russell, C. T., Steinberg, J. T., Chao, J. K., Zastenker, G., ... Kawano, H. (1998). Magnetopause location under extreme solar wind conditions. *Journal of Geophysical Research: Space Physics*. doi: 10.1029/98ja01103
- Song, P., & Russell, C. T. (1992). Model of the formation of the low-latitude boundary layer for strongly northward interplanetary magnetic field. *Journal of Geophysical Research*. doi: 10.1029/91ja02377
- Sorathia, K. A., Merkin, V. G., Ukhorskiy, A. Y., Allen, R. C., Nykyri, K., & Wing, S. (2019). Solar Wind Ion Entry Into the Magnetosphere During Northward IMF. *Journal of Geophysical Research: Space Physics*. doi: 10.1029/2019JA026728
- Stenuit, H., Fujimoto, M., Fuselier, S. A., Sauvaud, J. A., Wing, S., Fedorov, A., ... Pedersen, A. (2002). Multispacecraft study on the dynamics of the dusk-flank magneto-

- sphere under northward IMF: 10-11 January 1997. *Journal of Geophysical Research: Space Physics*. doi: 10.1029/2002JA009246
- Stenuit, H., Sauvaud, J. A., Delcourt, D. C., Mukai, T., Kokubun, S., Fujimoto, M., ... Lepping, R. P. (2001). A study of ion injections at the dawn and dusk polar edges of the auroral oval. *Journal of Geophysical Research: Space Physics*. doi: 10.1029/2001ja900060
- Stone, E. C., Frandsen, A. M., Mewaldt, R. A., Christian, E. R., Margolies, D., Ormes, J. F., & Snow, F. (1998). The Advanced Composition Explorer. *Space Science Reviews*, 86(1), 1–22. Retrieved from <https://doi.org/10.1023/A:1005082526237> doi: 10.1023/A:1005082526237
- Takagi, K., Hashimoto, C., Hasegawa, H., Fujimoto, M., & TanDokoro, R. (2006). Kelvin-Helmholtz instability in a magnetotail flank-like geometry: Three-dimensional MHD simulations. *Journal of Geophysical Research: Space Physics*. doi: 10.1029/2006JA011631
- Taylor, M. G., & Lavraud, B. (2008). Observation of three distinct ion populations at the Kelvin-Helmholtz-unstable magnetopause. *Annales Geophysicae*. doi: 10.5194/angeo-26-1559-2008
- Terasawa, T., Fujimoto, M., Mukai, T., Shinohara, I., Saito, Y., Yamamoto, T., ... Lepping, R. P. (1997). Solar wind control of density and temperature in the near-Earth plasma sheet: WIND/GEOTAIL collaboration. *Geophysical Research Letters*. doi: 10.1029/96GL04018
- Tóth, G., Sokolov, I. V., Gombosi, T. I., Chesney, D. R., Clauer, C. R., De Zeeuw, D. L., ... Kóta, J. (2005). Space weather modeling framework: A new tool for the space science community. *Journal of Geophysical Research: Space Physics*. doi: 10.1029/2005JA011126
- Tóth, G., van der Holst, B., Sokolov, I. V., De Zeeuw, D. L., Gombosi, T. I., Fang, F., ... Opher, M. (2012). Adaptive numerical algorithms in space weather modeling. *Journal of Computational Physics*. doi: 10.1016/j.jcp.2011.02.006
- Tsyganenko, N. A., & Stern, D. P. (1996). Modeling the global magnetic field of the large-scale Birkeland current systems. *Journal of Geophysical Research: Space Physics*. doi: 10.1029/96ja02735
- Varsani, A., Nakamura, R., Sergeev, V. A., Baumjohann, W., Owen, C. J., Petrukovich, A. A., ... Ergun, R. (2017). Simultaneous Remote Observations of Intense Reconnection Effects by DMSP and MMS Spacecraft During a Storm Time Substorm. *Journal of Geophysical Research: Space Physics*. doi: 10.1002/2017JA024547
- Wang, C. P., Fuselier, S. A., Hairston, M., Jia Zhang, X., Zou, S., Avakov, L. A., ... Bortnik, J. (2019). Event Studies of O<sup>+</sup> Density Variability Within Quiet-Time Plasma Sheet. *Journal of Geophysical Research: Space Physics*. doi: 10.1029/2019JA026644
- Wang, C. P., Lyons, L. R., Nagai, T., Weygand, J. M., & Lui, A. T. (2010). Evolution of plasma sheet particle content under different interplanetary magnetic field conditions. *Journal of Geophysical Research: Space Physics*. doi: 10.1029/2009JA015028
- Wing, S., Johnson, J. R., Newell, P. T., & Meng, C. I. (2005). Dawn-dusk asymmetries, ion spectra, and sources in the northward interplanetary magnetic field plasma sheet. *Journal of Geophysical Research: Space Physics*. doi: 10.1029/2005JA011086
- Zwolakowska, D., Koperski, P., & Popielawska, B. (1992). Plasma populations in the tail during northward IMF. *Proceedings of the international conference on substorms (ICS-1), Kiruna, Sweden (ESA SP-335)*, 57–62.
- Zwolakowska, D., & Popielawska, B. (1992). Tail Plasma Domains and the Auroral Oval — Results of Mapping Based on the Tsyganenko 1989 Magnetosphere Model. *Journal of Geomagnetism and Geoelectricity*(44), 1145–1158. doi: 10.5636/jgg.44.1145